# Stability Analysis of Masonry Domes and Crack Interpretation Through a 3D-Rigid-Block Model with Concentrated Deformability

Stefano Galassi[1,2(✉)] and Giacomo Tempesta[1]

[1] Department of Architecture, University of Florence, Florence, Italy
stefano.galassi@unifi.it

[2] Department of Mediterranean Architecture Research Center, Faculty of Applied Sciences, Catholic University "Our Lady of Good Counsel" of Tiranë, Tiranë, Albania

**Abstract.** The preservation of buildings belonging to architectural heritage is a topic that is very close to society's heart. They are mainly constructed of load-bearing masonry and feature typical architectural and structural components such as arches, colonnades, vaults and domes. These components often have cracks and, in some cases, an extensive crack pattern can even be observed. Cracking is a common occurrence in masonry structures, given the very low tensile strength of the mortar joints used to bind the masonry units. What really matters is determining the causes to prevent local or global collapse and to design appropriate reinforcement measures. To this purpose, structural analyses must be performed. Therefore, targeted mechanical models and analysis methods must be developed. This paper focuses especially on domes, for the analysis of which methods based on graphic statics were developed in the past. According to them, a dome was analyzed as a series of meridian slices acting as individual arches and the stability was assessed using the thrust line method. The advent of elasticity theory in the 19$^{th}$ century introduced new methods of analysis, such as the membrane theory; however, this theory is not particularly suitable for the study of masonry domes because, to satisfy the equilibrium conditions, it also considers tensile stresses along the lower parallels. In this paper, a 3D-Rigid-block model with concentrated deformability is presented. The deformability is concentrated in the joints, to which a no-tension behavior or a low threshold strength can be assigned. This model can predict the occurrence of cracks in joints and, consequently, interpret their cause. Its reliability is demonstrated by the analysis of a well-known and much-debated case study.

**Keywords:** Domes · Masonry · No-Tension · Nonlinear Analysis · Stability · Crack Interpretation

## 1 Introduction

Every country has historic buildings that tell the story of its origins. Italy is the country with the highest concentration of historical and architectural heritage in the world [1]. Most of the historic building stock consists of masonry buildings, some of which are

© The Author(s), under exclusive license to Springer Nature Switzerland AG 2027
O. Gervasi et al. (Eds.): ICCSA 2026 Workshops, LNCS 16758, pp. 533–550, 2027.
https://doi.org/10.1007/978-3-032-30497-1_32

in ruins and others merely damaged; they are characterized by typical architectural and structural elements, such as arches, vaults, domes, spiral stairs, etc. We must preserve these architectural structures as a tribute to our past. To preserve them, we need to assess their stability based on reliable analysis methods [2–20].

As regards to masonry domes – the subject of this paper – the first significant analysis methods based on equilibrium date back to the 18$^{th}$ century, with the publication of numerous memoirs by the Royal Academy of Sciences in Paris. We denote the set of this 18$^{th}$ century memoirs as the "first school of thought", to distinguish it from the changed way of thinking that emerged in the 19$^{th}$ century.

We can identify Pierre Bouguer [21] as the leading figure of this early school of thought, which interprets the behavior of a dome as a set of independent, arch-shaped structural elements. According to this theory, the stability of a dome is assessed by analyzing the stability of these one-dimensional elements, which can be done by identifying a line of thrust that lies entirely within their profile using the principles of graphic statics. It is worth noting that this interpretation of the mechanical behavior of a dome corresponds to that of Poleni [22] who analyzed in 1734 the stability of San Peter's dome in Rome as an assemblage of "solid sectors". Even the analysis of a dome divided into a series of "orange slices" – which Heyman [23] proposed in the 1960s in the context of limit analysis and which assumes the absence of forces along the dome's parallels, i.e. of interactions between these arched elements – can also be traced back to these earlier interpretations.

Bouguer's studies cover both the design of a new dome and the structural analysis of an existing dome. In his memoir, the first subject is referred to as the "first question" and concerns determining the best shape for a dome capable of supporting its own weight. He was the first to propose the equation of the funicular meridian as the solution to this problem: the best shape for the dome is achieved by modelling the curve of the meridian so that it coincides with the funicular curve of the own weight of a slice of the dome. The second subject, instead, is called the "second question" and concerns the stability analysis of an existing dome. Even if he did not provide the mathematical solution to this problem, he realized that the stress state inside a dome is two-dimensional and, consequently, introduced the topic of two-dimensional behavior.

The subject of the two-dimensional behavior of the dome was developed in depth in the 19$^{th}$ century, with the advent of the theory of elasticity. The most famous method developed in this period and in this context is the one called "membrane theory", devised by E. Beltrami [24]. Even if this method was originally conceived to analyze membranes, it was also applied from the very beginning to the analysis of masonry domes despite the latter do not behave like membranes. In fact, according to this theory, the internal forces in a dome are axial compressive forces along the meridians, with values increasing from the crown to the base, and axial forces along the parallels which have different signs: they are compressive on the upper parallels and tension on the lower ones. The position of the parallel that marks the transition from compression to the tension forces, referred to as the neutral parallel, depends only on the shape of the dome.

This scenario of internal forces is generally not consistent with the one that a masonry dome can withstand, because it is not as thin as a membrane and has a very low tensile strength. Tensile forces cause the development of cracks along the meridians, the internal

forces are no longer located in the middle surface of the dome and the position of the neutral parallel is variable and depends on these aspects. Based on this reasoning, H. T. Eddy in 1878 [25] and M. Lévy [26] in 1888 proposed, independently of each other, two very similar graphical methods to assess the stability of a masonry dome based on the assumption that the dome has a double behavior: the portion above the neutral axis has a two-dimensional behavior, characterized by compressive forces both along the meridians and the parallels; instead, below the neutral parallel the dome splits into a series of meridian arches caused by the tensile forces along the lower meridians and, therefore, the lower portion of the dome behaves as a set of independent one-dimensional structures. These graphical methods allow one to identify the position of the neutral parallel and draw the thrust line at the bottom [27].

All these methods have a common feature: they are based only on equilibrium because, as is known, masonry structures collapse due to lack of stability, which is determined by the geometric shape of the structure and the unilateral no-tension nature of the material, rather than to the material's failure due to exceeding its strength thresholds. Accordingly, thrust line methods, originally formalized by Gerstener [28], have been extended to the analysis of three-dimensional masonry structures, such as vaults and domes, using thrust networks. Thrust network analysis, based on Heyman's assumptions, was originally developed by O'Dwyer [29], fully developed by Block and Ochsendorf [30] and then reformulated and extended by Marmo and Rosati [31]. It consists in identifying a network of only compressive forces within the boundary of masonry to ensure stability. However, it does not give any additional information about the level of stability. To compute the level of stability, this method has further been extended in [32] exploiting the concept of geometrical factor of safety proposed by Heyman.

However, this approach, which is framed in the context of limit analysis under Heyman's assumptions, can lead to overestimate the load-bearing capacity. To overcome this issue, many authors proposed methods to account for a finite compressive strength and stereotomy [33, 34], and the most recent paper found in the literature is that of Aita [35, 36], who uses a numerical approach based on the force density method.

In this paper, instead, to analyze the stability of masonry domes a three-dimensional rigid-block model with deformability concentrated at joints is proposed. Joints along the parallels and the meridians are modelled as discrete devices consisting of a set of axial and shear links, the former are arranged orthogonally to the middle plane of the joints and the latter are arranged within it along the meridians and parallels. Material nonlinearity is considered by incorporating failure criteria for the axial compressive and tensile links as well as for the shear links. The nonlinear numerical procedure that handles the static and elastic-kinematic analysis of this model uses Somigliana distortions to satisfy the failure criteria. The failure of the links that do not meet the failure criteria allows one to detect the occurrence of cracks in the joints and to draw the deformed configuration of the structure. The reliability of the proposed procedure is demonstrated by the stability analysis of the dome of Santa Maria del Fiore in Florence (Italy) and by the comparison between the numerically predicted crack pattern and the one observed in the existing dome. The computer program *BrickWORK 2.0* has been developed to create the structural model of the dome and automatically perform the analysis.

## 2 Numerical Approach

### 2.1 Mechanical Model

The model of the masonry dome consists of a set of rigid blocks, cut out between two adjacent meridians and parallels. Except for specific cases, these are mainly rigid hexahedral elements. They are connected to one other by meridian and parallel joints, which act as thin elastic layers. By doing so, this structural model is defined as "rigid block model with concentrated elasticity" and, accordingly, it is governed by equilibrium equations of blocks and congruency equations of joints. Let $n$ and $m$ denote the overall number of blocks and joints, respectively (Fig. 1).

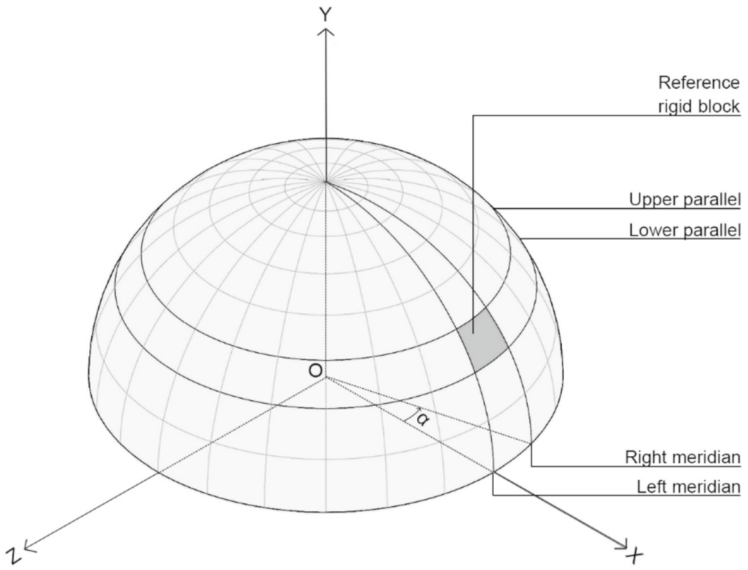


**Fig. 1.** Discrete model of the dome.

According to Drucker, joints are modelled through a discrete device consisting of a set of links orthogonal to the middle plane of the joint, to transfer the axial force between the blocks, and a set of links lying on it to transfer the shear force (Fig. 2). The greater the number of axial and shear links, the more refined the model and the more accurate the results, particularly with regard to the calculation of cracks. It is worth noting that the number of shear links is twice that of the axial links. We denote the number of axial links by $k$. The reason for it is that every point $i$ of the joint (with $1 \leq i \leq k$) connecting two adjacent blocks must transfer three internal forces to prevent internal instability: the axial force and two shear forces acting along two different directions within the middle plane of the joint. Accordingly, the simplest device of the joint consists of four axial links, at the four vertices of the middle plane of the joint to connect two adjacent blocks, two shearing links along the upper and lower parallel and two shearing links along the

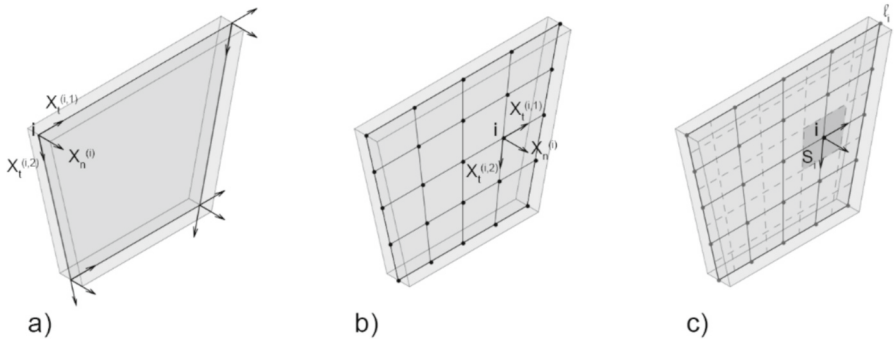


**Fig. 2.** Discrete model of the joint device: in a) the simplest device; in b) a more refined device; in c) cross-sectional area and length of the i-th link.

left and right meridian. In Fig. 2a, which shows this device, the links are replaced by the internal forces associated with them.

In Fig. 2b, instead, a more refined joint device is shown. This is achieved by further discretizing the simple device shown in Fig. 2a, by subdividing the four edges of the middle plane of the joint into three equal segments which identify four nodes on each edge. By connecting these, a network of 16 nodes is created. At each node there is an axial and two shear links. The axial link passing through the node is perpendicular to the middle plane. The directions of the shear links are those of the parallel and the meridian passing through the node.

### 2.2 Behavior of the Joints

Joints are designed as thin, elastic layers inserted between the rigid blocks that make up the structure. However, a distinction must be made between compression and tensile deformation in order to accurately reproduce the actual properties of the masonry. Accordingly, different strength criteria are assigned to the axial and shear links of the joint device.

Axial links may be assigned either an infinite compression strength if a linear-elastic behavior is assumed (Fig. 3a) or a limit threshold strength corresponding to the crushing of masonry if a linear-elastic-perfectly plastic behavior is adopted (Fig. 3b). With regard to tension, a no-tension material may be adopted but a limit threshold strength can also be considered that causes the failure of the link and the occurrence of a crack if a linear elastic-rigid behavior is assumed under tension (Fig. 3a,b). Shear links, instead, may be assigned either an infinite shear strength to prevent sliding if a linear-elastic behavior is assumed (Fig. 3c) or a limit threshold strength which can result in two different effects: the failure of that link if a linear-elastic-brittle behavior is adopted (Fig. 3d); its yielding in case of a linear-elastic-perfectly plastic behavior (Fig. 3e).

It is worth noting that the tensile failure of an axial link involves also the failure of the two shear-links associated with it in order for the crack to occur, but not vice versa. In this way, sliding occurs without dilatancy because the axial link maintains its axial force.

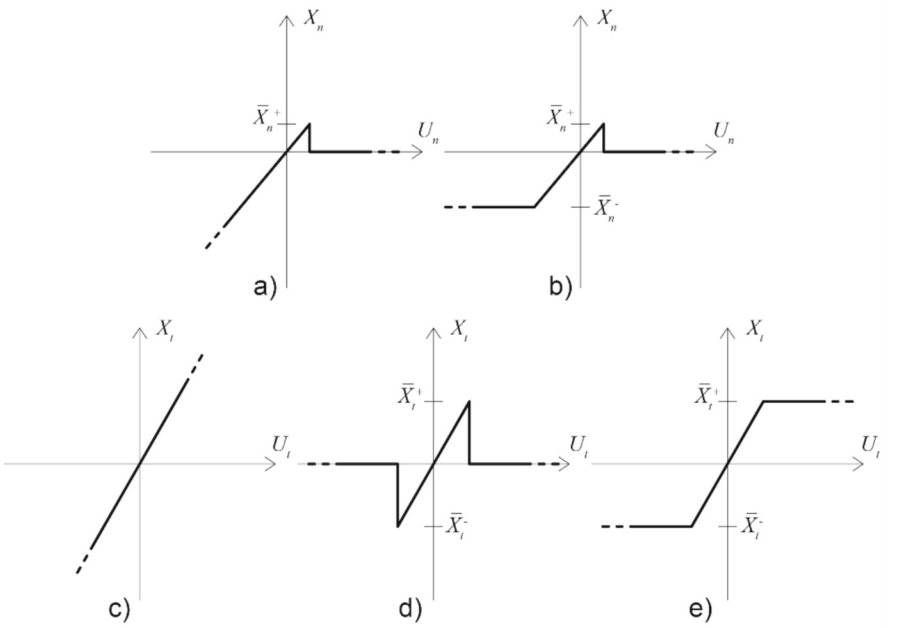


**Fig. 3.** Mechanical behavior of the joint axial links with finite tensile strength and infinite (a) or finite (b) compressive strength; joint shear links with (c) infinite strength or a threshold strength value causing the failure (d) or its yielding (e).

### 2.3 Problem Setting

To analyze the discrete model of the dome shown in Fig. 1 and Fig. 2, the equilibrium equations of rigid blocks and the elastic-kinematic equations of joints are formulated. The overall system of linear equations that is obtained is written in matrix form in Eq. 1:

$$\begin{cases} AX + F = 0 \\ \tilde{A}U + KX = \Delta \end{cases} \tag{1}$$

In the first equation, that describes the equilibrium condition, $F$ is the load vector, $X$ is the vector of the axial and shear forces within the links of the joint device to be calculated and $A$ is the matrix of its coefficients.

In the second equation, $\tilde{A}$ is the kinematic matrix and it is the transpose of the equilibrium matrix $A$ according to the static-kinematic duality, $U$ is the vector of the displacements of the block centroids and its entries are the horizontal displacements along the x and z axes, the vertical displacement along the y axis and the three rotations about the x, y and z axes. Matrix K is a square diagonal matrix and its entries $k_{i,i} = \frac{\ell_i}{E \cdot S_i}$ are the deformability coefficients of the joint links. In detail, $\ell_i$ is the length of the i-th link of the joint device, $S_i$ its sectional area and $E$ the Young's modulus of the joint (Fig. 2c). Finally, vector $\Delta$ is denoted as "distortion vector" and its purpose is twofold in the numerical procedure:

- to ensure that the axial and shear forces in the links meet the specified failure criteria;

- to ensure compatibility even when some links fail and cracks develop.

Therefore, vector $\Delta$ is partitioned into the sub-vector $\Delta^*$ to address the first issue and the sub-vector $\Delta^{**}$ to address the second.

For the purposes of the analysis, the failure criteria described in Sect. 2.2 and associsated with the specific behaviour of the axial and shear links shown in Fig. 3, are formulated in Eq. 2:

$$\begin{cases} \overline{X}_n^{-(i)} \leq X_n^{(i)} \leq \overline{X}_n^{+(i)} \\ \left|X_t^{(i)}\right| \leq \left|\overline{X}_t^{(i)}\right| = |c| + \mu \cdot \left|X_n^{(i)}\right| \end{cases} \tag{2}$$

where the vector of internal forces is partitioned into the sub-vector $X_n$ of the axial forces and the sub-vector $X_t$ of the shear forces to properly handle the relevant failure criteria.

The first inequality of Eq. 2 sets the threshold compressive strength $\overline{X}_n^{-(i)}$ and the threshold tensile strength $\overline{X}_n^{+(i)}$ for the axial force $X_n^{(i)}$ of the i-th link. It goes without saying that to define a no-tension material, one simply sets $\overline{X}_n^{+(i)} = 0$ and to define a marerial with infinite compression strength one sets $\overline{X}_n^{-(i)} = -\infty$.

The second inequality describes the frictional behavior of the joint with non-associated flow rule. According to the Coulomb strength criterion, the shear force $X_t^{(i)}$ of the i-th link, computed as the vector sum of the shear force $X_t^{(i,1)}$ along the parallel and the shear force $X_t^{(i,2)}$ along the meridian passing through point $i$, must not exceed the threshold value, given by the sum of the friction force $\mu \cdot X_n^{(i)}$ and the cohesion $c$ to prevent sliding. In the second inequality of Eq. 2, $\mu$ is the friction factor of the joint and $X_n^{(i)}$ is the axial force acting at point $i$. Refer to Fig. 2 for the nomenclature.

These failure criteria imply nonlinear behaviour of the masonry dome. Accordingly, a nonlinear numerical procedure, that works as follows, is developed:

- First, the vector of internal forces X, corresponding to the linear-elastic static solution of the problem, is calculated by solving Eq. 1. We denote this vector $X_0$. Therefore, at the starting point of the analysis, we have $X = X_0$;

- Then, this vector is partioned into the sub-vectors $X_n$ and $X_t$ to check if the axial and shear forces meet the corresponding failure criteria set in Eq. 2. If some entries do not meet them, distoritons $\Delta^*$ are introduced, iteratively, in the link where the internal force exceeds its threshold value the most. Therefore, this is an iterative procedure.

Specifically, referring to Fig. 3a and Fig. 3b, the distortion introduced in an axial link subjected to a tensile force exceeding the tensile threshold value $\overline{X}_n^+$, nullifies the internal force and causes the failure of that link and the associated shear links along the parallel and meridian, as well as the development of a crack. Furthermore, referring to Fig. 3b, the distortion introduced in an axial link subjected to a compression force exceeding the compression threshold value $\overline{X}_n^-$, sets the internal forces to that value and causes the yielding of that link.

Figures 3d and 3e show, instead, the effect of distortions on the shear links along the parallels and meridians. In detail, if the shear behavior in Fig. 3d is adopted, the distortion introduced in a shear link subjected to a shear force exceeding the threshold

value $\overline{X}_t$, nullifies the internal force and causes the failure of that link. Convesely, if we consider the shear behavior shown in Fig. 3e, the distortion sets the internal forces to the threshold value and causes the yielding of that link. In both cases, sliding occurs. It is worth noting that if the behavior shown in Fig. 3c is assumed, distortions are never introduced in the shear links and sliding is prevented.

In the forthcoming sections of the paper, the numerical procedure is described in detail, discussing first the static analysis, then the elastic-kinematic analysis.

### 2.4 Calculation of Internal Forces

By solving Eq. 1 in accordance with the failure criteria expressed by Eq. 2, we obtain the vector $X$ of the internal forces within the axial and shear links of the joint device:

$$X = -K^{-1}\tilde{A}R^{-1}F + K^{-1}\left(I - K^{-1}\tilde{A}R^{-1}A\right)\Delta^* \tag{3}$$

It can be noticed that this vector is given by the sum of two vectors, respectively shown in Eq. 4 and Eq. 5:

$$X_0 = -K^{-1}\tilde{A}R^{-1}F \tag{4}$$

$$X_\perp = K^{-1}\left(I - K^{-1}\tilde{A}R^{-1}A\right)\Delta^* \tag{5}$$

In Eqs. 3 to 5, matrix $R = AK^{-1}\tilde{A}$ is the stiffness matrix of the structure.

The vector $X_0$ is the linear-elastic solution obtained by setting $\Delta^* = 0$ and solving Eq. 1. The vector $X_\perp$, on the other hand, is the solution of Eq. 1 that can be obtained by setting vector $F = 0$, assuming that there are two separate static problems: the dome subject only to the dead loads $F$ and the dome subject only to the distortions $\Delta^*$. However, the two problems are closely linked, as the distortions are aimed at meeting the failure criteria in Eq. 2. For this reason, it is observed that it is not possible to calculate the distortion vector $\Delta^*$ before calculating the static solution vector $X$, but also the latter is a function of the former (see Eq. 3). It is like a dog biting its own tail. To get around this trouble, a numerical workaround has been devised, as illustrated in the equations below.

By defining the distortion matrix D as follows:

$$D = K^{-1}\left(I - K^{-1}\tilde{A}R^{-1}A\right) \tag{6}$$

Equation 5 is re-written, in a more concise way, in the form of Eq. 7:

$$X = X_0 + D\Delta^* \tag{7}$$

Next, matrix D and vectors $X$, $X_0$ and $\Delta^*$ are partitioned in such a way as to separate entries that meet the failure criteria from those that do not. We denote the former by the subscript $b$ and the latter by the subscript $c$. With this in mind, Eq. 7 is partitioned as follows:

$$\begin{bmatrix} X_b \\ T \end{bmatrix} = \begin{bmatrix} X_{0b} \\ X_{0c} \end{bmatrix} + \begin{bmatrix} D_b & B \\ \tilde{B} & D_c \end{bmatrix} \cdot \begin{bmatrix} 0 \\ \Delta_c^* \end{bmatrix} \tag{8}$$

In Eq. 8, the final static solution vector X is composed of two sub-vectors: the sub-vector $T$ that is populated by the axial and shear forces modified by the distortions introduced to meet the failure criteria, whilst the sub-vector $X_b$ consists of the internal forces that do not require distortions to satisfy the criteria.

Entries of sub-vector $T$ are defined in Eq. 9, depending on the failure critera adopted for the i-th axial or shear link:

$$t_i = \begin{cases} \overline{X}_n^{+(i)} \\ \overline{X}_n^{-(i)} \\ \overline{X}_t^{(i)} = 0 \\ \overline{X}_t^{(i)} = c + \mu \cdot X_n^{(i)} \end{cases} \tag{9}$$

The first and the second terms of Eq. 9 relate to the first failure criterion in Eq. 2 for the axial links. In particular, the first one refers to a no-tension axial link (Fig. 3a and Fig. 3b) and the second one to the yielding of an axial compressed link (Fig. 3b).

The third and the fourth terms of Eq. 9 relate to the second failure criterion in Eq. 2 for the shear links. Specifically, the third one refers to the elastic-rigid behavior shown in Fig. 3d whilst the fourth refers to the elastic-plastic behavior shown in Fig. 3e.

The solution to Eq. 8 provides precisely the sub-vector $\Delta_c^*$ (Eq. 10), consisting of the non-zero entries of the distortion vector $\Delta^*$ aimed at satisfying the failure criteria and, subsequently, the sub-vector $X_b$ (Eq. 11), consisting of the entries of vector X that have been indirectly influenced by the distorsions introduced in other links:

$$\Delta_c^* = D_c^{-1}(T - X_{0c}) \tag{10}$$

$$X_b = X_{0b} + \mathrm{B}D_c^{-1}(T - X_{0c}) \tag{11}$$

We refer to the sub-vector $\Delta_c^*$ as the "vector of effective distortions".

### 2.5 Displacements and Crack Pattern

The second phase of the analysis involves calculating the displacement of the blocks, as well as the deformation and propagation of cracks along the joints.

To draw the displaced configuration of the dome, it is necessary to calculate the displacements of the eight vertices of the blocks. They are computed in function of the displacements of the block centroids.

The latter could be computed by directly solving Eq. 1 only if the internal forces do not exceed their threshold values expressed by the failure conditions in Eq. 2. In this specific case the vector of the displacement of block centroids corresponds to the linear-elastic solution and is expressed by Eq. 12:

$$U = \mathrm{R}^{-1}\left(F + \mathrm{A}K^{-1}\Delta\right) \tag{12}$$

However, Eq. 12 does not hold when some of the links in the joint device fail or yield plastically, resulting in cracks or slippage. To take these occurrences into account,

we apply the same numerical workaround to the elastic-kinematic equation as we used previously for the equilibrium equation. In this case, distortions $\Delta^{**}$ are introduced to restore the compatibility that has been altered by the cracks and slippage. Consequently, the second of Eq. 1 is partitioned to distinguish between entries that have been directly altered by the distortions $\Delta^{**}$ introcuced and those that have been changed only as a result:

$$\begin{bmatrix} \sim & & \\ \mathrm{A_b} & \mathrm{K_b} & 0 \\ \sim & & \\ \mathrm{A_c} & 0 & \mathrm{K_c} \end{bmatrix} \begin{bmatrix} \overline{U} \\ \mathrm{X_b} \\ 0 \end{bmatrix} = \begin{bmatrix} 0 \\ \Delta_c^{**} \end{bmatrix} \tag{13}$$

The solution to Eq. 13 provides precisely the vector $\overline{U}$ of effective displacements of block centroids and, consequently, the sub-vector $\Delta_c^{**}$, consisting of the non-zero entries of the distortion vector $\Delta^{**}$ aimed at restoring compatibility.

$$\overline{\mathrm{U}} = -\mathrm{A_b}(\tilde{\mathrm{A}}_\mathrm{b}\mathrm{A_b})^{-1}(\mathrm{K_b}\mathrm{X_b}) \tag{14}$$

$$\Delta_c^{**} = \overset{\sim}{\mathrm{A}}_\mathrm{c}\overline{\mathrm{U}} \tag{15}$$

Note that vector $\overline{U} \neq U$ and entries of vector $\Delta_c^{**}$ represent the width of cracks at the joint links and, therefore, allow the crack pattern to be determined.

Finally, the new coordinates of the block vertices can be determined based on the six displacements of the block centroids stored in the vector $\overline{\mathrm{U}}$.

Considering the j-th vertex P of the i-th block (denoted by $P_j^{(i)}$, with $1 \leq j \leq 8$, $1 \leq i \leq n$), the six displacements of the block centroid are referred as $u_{xG}^{(i)}$, $u_{yG}^{(i)}$, $u_{zG}^{(i)}$, $\varphi_{G,x}^{(i)}$, $\varphi_{G,y}^{(i)}$, $\varphi_{G,z}^{(i)}$ and the new coordinates of the displaced position of the vertex $P_j'^{(i)}$ are calculated, according the rules of finite kinematics, using the matrix Eq. (16):

$$\begin{Bmatrix} x'^{(i)}_{P_j} \\ y'^{(i)}_{P_j} \\ z'^{(i)}_{P_j} \end{Bmatrix} = \begin{Bmatrix} u_{x_G}^{(i)} \\ u_{y_G}^{(i)} \\ u_{z_G}^{(i)} \end{Bmatrix} + \begin{bmatrix} 1 & 0 & 0 \\ 0 & cos\varphi_{G,x}^{(i)} & -sin\varphi_{G,x}^{(i)} \\ 0 & sin\varphi_{G,x}^{(i)} & cos\varphi_{G,x}^{(i)} \end{bmatrix} \cdot \begin{bmatrix} cos\varphi_{G,y}^{(i)} & 0 & sin\varphi_{G,y}^{(i)} \\ 0 & 1 & 0 \\ -sin\varphi_{G,y}^{(i)} & 0 & cos\varphi_{G,y}^{(i)} \end{bmatrix} \cdot \begin{bmatrix} cos\varphi_{G,z}^{(i)} & -sin\varphi_{G,z}^{(i)} & 0 \\ sin\varphi_{G,z}^{(i)} & cos\varphi_{G,z}^{(i)} & 0 \\ 0 & 0 & 1 \end{bmatrix} \cdot \begin{Bmatrix} x_{P_j}^{(i)} \\ y_{P_j}^{(i)} \\ z_{P_j}^{(i)} \end{Bmatrix} \tag{16}$$

This equation can also be written in a shorter, more compact form using Eq. 17:

$$P\prime = \overline{\mathrm{U}}_i + \left(\mathrm{R_x}\mathrm{R_y}\mathrm{R}_z\right)P \tag{17}$$

In Eq. 16 and Eq. 17, $\mathrm{R_x}$, $\mathrm{R_y}$ and $\mathrm{R_z}$ are the rotation matrices about the x, y and z axes calculated from the angles $\varphi_{G,x}^{(i)}$, $\varphi_{G,y}^{(i)}$, $\varphi_{G,z}^{(i)}$, respectively, and entries of the sub-vector $\overline{\mathrm{U}}_i = \left\{ u_{xG}^{(i)} \; u_{yG}^{(i)} \; u_{zG}^{(i)} \right\}$. of vector $\overline{\mathrm{U}}$ are the displacements along the x, y and z axes of the centroid G of the i-th block.

### 2.6 *BrickWORK* Software-Aided Modelling

To analyze 3D-structures made of rigid blocks with deformability concentrated at joints, the computer program *BrickWORK* [37–40] has been extended. With this new release,

*BrickWORK 2.0* is equipped with a graphical user interface (GUI) that allows one to easy create 3D-models obtained by the extrusion of a plane profile along a straight or a circular line.

To create a dome model, a series of rigid blocks, positioned at the spacing of the radial joints (those that will form the joints along the dome's parallels), is constructed along the directrix curve of the reference meridian in the Cartesian x, y plane. These rigid blocks can be drawn as closed polylines in a CAD environment and imported into *BrickWORK* as DXF vector file.

Next, using the "Joints" tool available in the software, the radial joints between the blocks and those at the base of the meridian are defined. The plane joint device is modelled as a set of links orthogonal to the bisector of the joint, to transfer the axial force between blocks, and a set of links along the bisector to transfer the shear force. The number of shear links is equal to the number of axial links. The simplest device of the joint consists of two axial links located at the upper and lower vertices of the middle plane of the joint (i.e. the bisector of the joint) connecting two adjacent blocks, and two shear links connecting the same points on the model (Fig. 4a). A more refined joint device (Fig. 4b) is obtained by dividing the joint's bisector into three equal segments which define four nodes. At each node there is one axial and one shear link. The latter device is particularly useful when the analysis aims to identify the crack pattern at the joints.

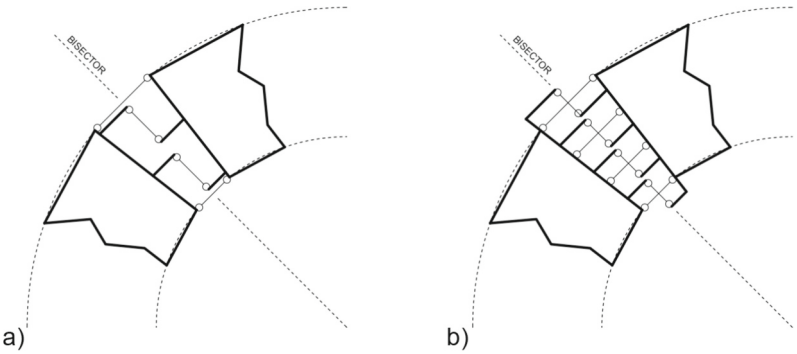


**Fig. 4.** Discrete model of the 2D-joint device: in a) the simplest device; in b) a more refined device.

This two-dimensional model is then extruded along a circular generatrix (Fig. 5) to form a full dome or a half-dome, such as that used to cover the apses of churches. To do this, *BrickWORK* provides a specific tool called "Create 3D model". This procedure requires the input of three parameters: the number $s$ of meridian slices to be created, the angular amplitude $\beta$ of the meridian joints between them and the angular amplitude $\alpha$ of the meridian slices measured along the circular generatrix (longitude), which comprises half the amplitude of the left and right meridian joints. It is worth noting that for a complete dome to form, $s \cdot \alpha$ must equal $2\pi$. Furthermore, it is also possible to divide the meridian slices into a series of sectors in order to refine the mesh of the rigid blocks, but also to create geometric models differing from the axially symmetric domes.

The extrusion algorithm transforms the plane rigid blocks into three-dimensional rigid blocks and the plane device that forms the radial joints shown in Fig. 4 into the three-dimensional device that forms the parallel joints shown in Fig. 2. At the same time, three-dimensional devices of the meridian joints are also being produced, of the same type as the devices arranged along the parallels.

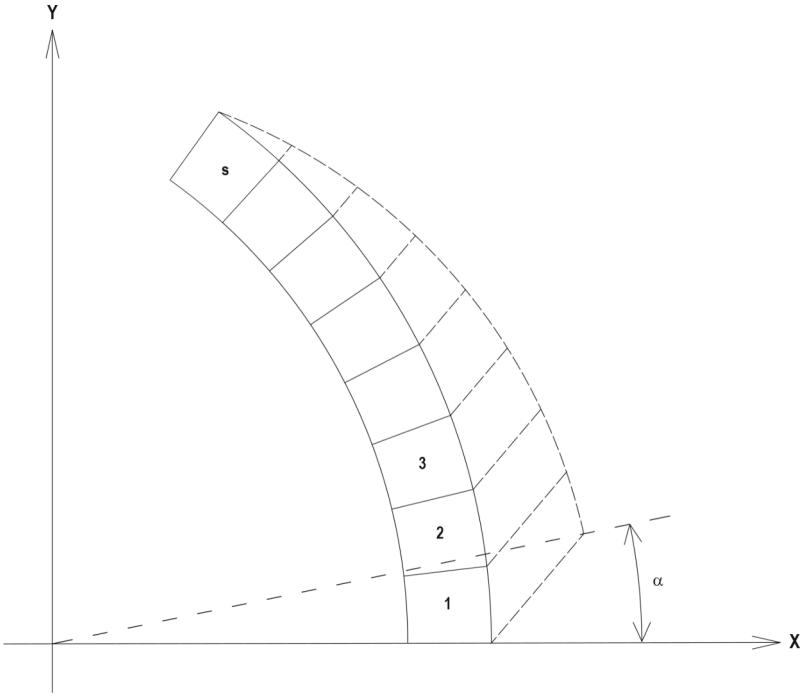


**Fig. 5.** Extrusion of the plane meridian profile to obtain the meridian slices that make up the three-dimensional model of the dome.

### 2.7 A Relevant Case Study

The numerical procedure presented in this paper has been used to analyze the stability of the Dome of Santa Maria del Fiore in Florence (Italy). *BrickWORK* 2.0 has been used to create the mechanical model of the dome and to perform the structural analysis.

The dome of Santa Maria del Fiore is an unusually shaped dome. Unlike typical axially symmetrical masonry domes, this is a polygonal dome built on an octagonal drum and crowned by an octagonal lantern (Fig. 6).

It was built between 1420 and 1436 by Filippo Brunelleschi, who won the competition for the dome of Santa Maria del Fiore, which was launched in 1418 in Florence by the Arte della Lana to resolve the issue of the cathedral's roof, which had remained unfinished.

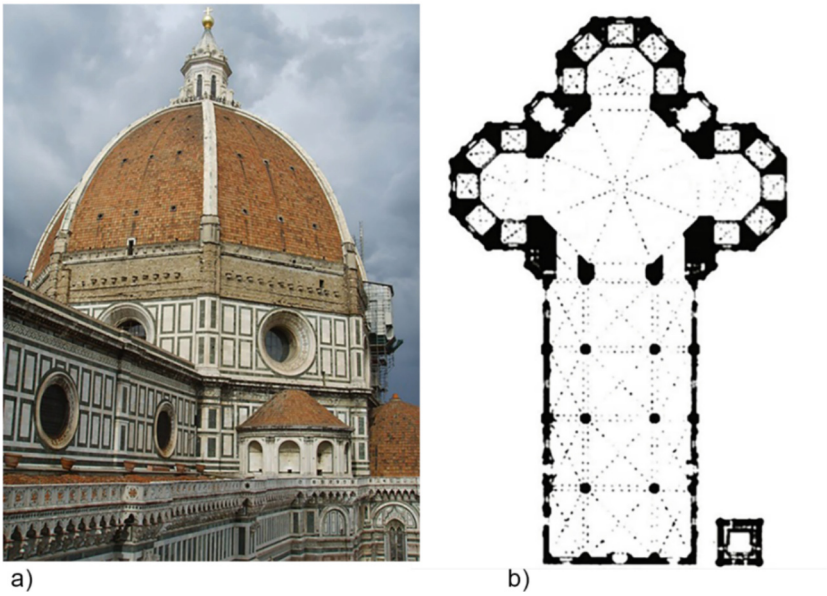


**Fig. 6.** Dome of Santa Maria del Fiore in Florence: a) picture; b) schematic plan.

The dome consists of two shells, one inner and one outer, separated by a cavity approximately 1.2 m wide that hosts the staircases leading to the lantern, and is composed of eight lunes that are segments of elliptical cylinders. The two shells are joined by a system of 24 meridian ribs (eight at the corners of the octagonal plan plus two per lune) and 10 parallel ribs.

The geometrical data used to create the mechanical model were derived from the pioneering studies by Salvatore di Pasquale published in 1977 [41] and they are shown in Fig. 7 together with the geometrical construction. This figure shows the octagonal plan of the dome (Fig. 7a), the cross sections of the dome drawn along the diagonal of the octagon (Fig. 7b) and at the middle of the octagon's sides (Fig. 7c). Please note that the shape has been regularized, as it is, in fact, an irregular octagon.

The profile of the diagonal rib of the inner shell is a circular curve whose radius, measuring 36 m, is 4/5 the inner diameter of the base. The inner and outer diameter are 45 and 54 m long, respectively; consequently, the overall thickness of the inner shell, the outer shell and the cavity between them is 4.5 m. Furthermore, the average thickness of the inner and the outer shell, taken at the middle of the lunes, is 2.20 and 0.90 m, respectively. Brunelleschi designed this pointed arch profile to give the dome greater height and make it more visible from the city.

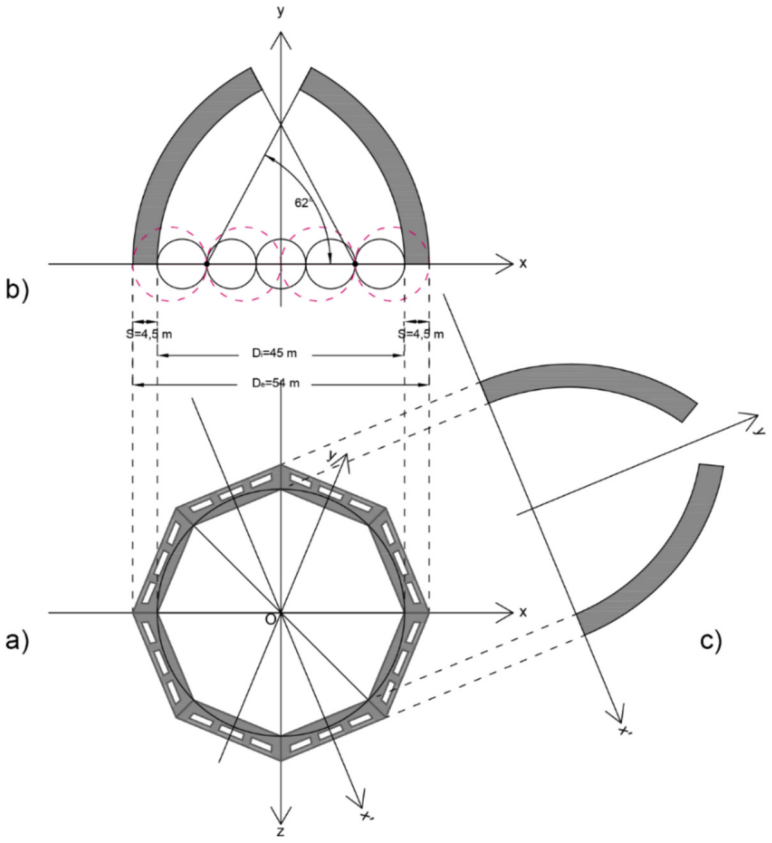


**Fig. 7.** Geometry: construction rules.

The three-dimensional mechanical model of the dome (Fig. 8) was constructed based on the shape of the meridian, which forms the circular rib. This consists of two parallel rows of 14 rigid blocks, the upper ones of which form the base of the lantern. For the assembly of the blocks, radial and meridian joints of minimum thickness were incorporated, consisting of devices comprising four axial and four shear links. The plane meridian was then extruded along a circular generatrix eight times at 45-degree intervals, so as to form a complete octagonal dome consisting of eight lunes. Each lune was also divided into eight sectors and, to create the eight corner ribs and the two ribs for each lune, some of the rigid blocks forming the outer structure were removed from the model. Finally, vertical point forces were applied to the upper blocks to simulate the weight of the lantern.

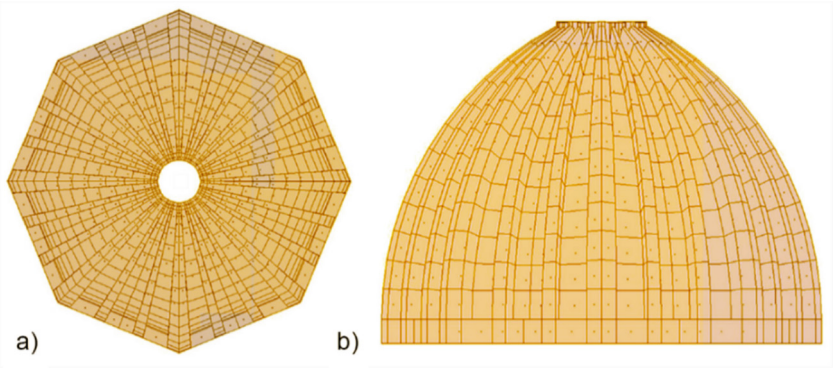


**Fig. 8.** Three-dimensional rigid block model of the dome of Santa Maria del Fiore: a) plan view; b) elevation view.

The analysis was carried out taking into account the axial behavior shown in Fig. 3a with a no-tension material and the shear behavior shown in Fig. 3c, thereby following Heyman's assumptions.

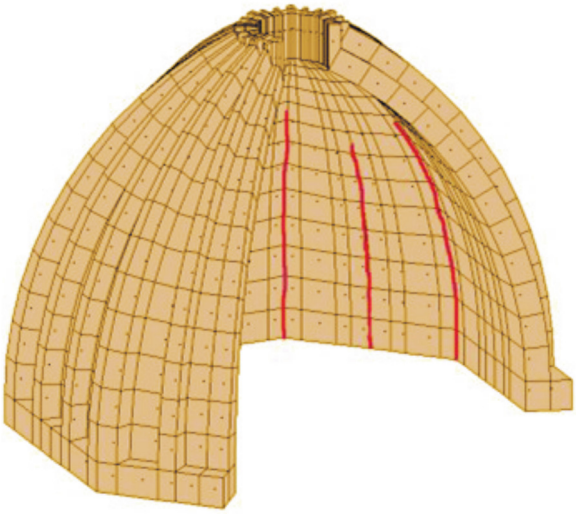

**Fig. 9.** Crack pattern predicted by the numerical procedure.

From the analysis, the dome is stable under the damage conditions illustrated in Fig. 9. The crack pattern, consisting of main meridional cracks along the big corner ribs and minor meridional cracks at the middle of the lunes, corresponds to that actually observed on the dome.

Furthermore, the compressive stresses are relatively low. At the base of the dome the predicted maximum compressive stress is 0.79 MPa at the major corner ribs, 0.78 MPa at the medium ribs and 0.47 MPa at the center of the lunes. These compression stresses

ensure that the strength criteria used in the analysis are consistent, as the crushing of the masonry can be disregarded.

It should also be noted that, unlike axially symmetric domes, in which shear forces are zero both along all parallels and meridians, in the case at hand the shear forces are zero only along the meridians at the big corner ribs and those at the middle of the lunes, which constitute the structure's only symmetry planes.

### 2.8 Conclusions

In this paper a three-dimensional rigid-block model with deformability concentrated at joints has been proposed to model masonry structures obtained using the extrusion procedure included in the software *BrickWORK 2.0*. The specific case of masonry domes was considered. Joints are represented by a discrete device consisting of links orthogonal to the middle plane of the joints, designed to transfer the axial force, and links lying within that plane, designed to transfer the shear force. For such links appropriate laws are formulated that describe the mechanical behavior together with the failure criteria. To address these criteria involving material nonlinearity, a nonlinear numerical procedure for stability analysis has been proposed, which uses Somigliana distortions to satisfy the failure criteria. The analysis of a significant case study, the dome of Santa Maria del Fiore in Florence (Italy), demonstrated the reliability of the proposed mechanical model and the numerical procedure to assess the stability of the structure and predict the crack pattern, which is consistent with that observed in the dome.

The extrusion procedure and the software developed enable the automatic modelling of structures that can be obtained by extruding a discrete planar model along a circular or straight line. Therefore, it is possible to model domes (complete, with hole and lantern, or on a drum), church apses, barrel and cloister vaults that include load-bearing walls. Further improvements will make it possible to model other types of structures that cannot be produced using extrusion processes, such as cross vaults.

Furthermore, the employment of Somigliana distortions offers a significant alternative to the traditional methods of variable stiffness matrix or linear programming, as it addresses nonlinear analysis using tools inherent to structural analysis rather than purely mathematical ones. On the contrary, as an iterative method is used, the computational cost can be significant. To reduce processing times, a single-step procedure is being developed to replace the current iterative procedure.

## References

1. Meloni, G., Pourfouladi, M., Pingaro, N.: Parametric modelling and nonlinear FE analysis of Trepponti bridge subjected to differential settlements. Buildings **16**(47), 1–20 (2026)
2. Pingaro, N., Buzzetti, M., Gandolfi, A.: A numerical strategy to assess the stability of curved masonry structures using a simple nonlinear truss model. Buildings **15**, 1–21 (2025)
3. Pingaro, N., Milani, G.: Simple interface element equipped with thickness for the non-linear static heterogeneous analysis of masonry walls in-plane loaded: implementation and validation. Eng. Struct. **351**, 122056 (2026)
4. Pingaro, N., Milani, G.: Simple non-linear numerical modelling of masonry arches reinforced with SRG using elasto-fragile and elasto-ductile truss finite elements. Eng. Struct. **293**, 116637 (2023)

5. Gandolfi, A., Pingaro, N., Milani, G.: Simple nonlinear numerical modeling for unreinforced and FRP-reinforced masonry domes. Buildings **14**(166), 1–21 (2024)
6. Gandolfi, A., Pingaro, N., Milani, G.: Elastic Body Spring Method (EBSM) for the stability analysis of the Global Vipassana Pagoda in Mumbai, India. Buildings **15**(653), 1–17 (2025)
7. Hua, Y., Buzzetti, M., Pingaro, N., da Silva, L.C.M., Milani, G.: A computerized tool for the kinematic limit analysis of 2D masonry structures failing on a tilting table. SoftwareX **30**, 102180 (2025)
8. Pingaro, N., Buzzetti, M., Milani, G.: Advanced FE nonlinear numerical modeling to predict historical masonry vaults failure: assessment of risk collapse for a long span cloister vault heavily loaded at the crown by means of a general-purpose numerical protocol. Eng. Fail. Anal. **167**, 109070 (2025)
9. Galassi, S., Tempesta, G.: Safety assessment of masonry undamaged and damaged arches subjected to gravitational loads and horizontal forces: a numeric procedure to identify the optimal thrust line. Int. J. Solids Struct. **301**, 112943 (2024)
10. Galassi, S.: An alternative approach for limit analysis of masonry arches on moving supports in finite small displacements. Eng. Fail. Anal. **145**, 107004 (2023)
11. Galassi, S., et al.: A numerical tool for assessing the effect of foundation settlements on the stability of masonry walls. In: Gusella, V., et al. (eds.) AID Monuments 2025 – Modello, interpretazione, Progetto. Lecture Notes in Civil Engineering, vol. 806, pp. 498–509. Springer, Cham (2026)
12. Cascini, L., Gagliardo, R., Portioli, F.: LiABlock_3D: a software tool for collapse mechanism analysis of historic masonry structures. Int. J. Archit. Herit. **14**(1), 75–94 (2020)
13. Paris, V., Gobbin, F., Nannei, V.M., Resmini, M., Mirabella Roberti, G.: Distinct element method analyses for damage assessment: the Northern Spur of Valverde Bulwark in the Venetian Fortress of Bergamo. Int. J. Archit. Herit. **19**(5), 687–701 (2025)
14. Iannuzzo, A., Mallardo, V.: A novel approach to model differential settlements and crack patterns in masonry structures. Eng. Struct. **323**, 119220 (2025)
15. Iannuzzo, A., Musone, V., Ruocco, E.: A neural network-based automated methodology to identify the crack causes in masonry structures. Comput. Aided Civ. Inf. **39**(24), 3769–3785 (2024)
16. Olivieri, C., Iannuzzo, A., Fortunato, A., DeJong, M.J.: The effect of concentrated loads on open-well masonry spiral stairs. Eng. Struct. **272**, 114952 (2022)
17. Iannuzzo, A., Gesualdo, A., Olivieri, C., Montanino, A.: 3D exploration of internal stresses due to lateral loads and foundation movements in a semicircular arch. In: M. Papadrakakis, M. Fragiadakis (eds.) 9th ECCOMAS Thematic Conference on Computational Methods in Structural Dynamics and Earthquake Engineering, pp. 2476–2491. Eccomas Procedia (2023)
18. Iannuzzo, A., Montanino, A.: A limit analysis-based CASS approach for the in-plane seismic capacity of masonry façades. Int. J. Solids Struct. **289**, 112633 (2024)
19. Cusano, C., Montanino, A., Olivieri, C., Paris, V., Cennamo, C.: Graphical and analytical quantitative comparison in the domes assessment: the case of San Francesco di Paola. Appl. Sci. **11**(8), 3622 (2021)
20. Cusano, C., Angjeliu, G., Montanino, A., Zuccaro, G., Cennamo, C.: Considerations about the static response of masonry domes: a comparison between limit analysis and finite element method. Int. J. Mason. Res. Innov. **6**(4), 502–528 (2021)
21. Bouguer, P.: Sur les lignes courbes qui sont propres à former les voûtes en dôme. Académie royale des sciences, Paris, pp. 149–66 (1734)
22. Poleni, J.: Memorie istoriche della gran cvpola del tempio vaticano e de' danni de essa, e de' ristoramenti loro, divise in libri cinqve, alla santità di nostro Signore papa Benedetto XIV. Nella Stamperia del Seminario, Padova (1748)
23. Heyman, J.: On shell solution for masonry domes. Int. J. Solids Struct. **3**(2), 227–241 (1967)

24. Beltrami, E.: Sull'equilibrio delle superfici flessibili ed inestensibili. Memorie dell'Accademia delle Scienze dell'Istituto di Bologna **4**(3), 217–265 (1882)
25. Eddy, H.T.: Researches in Graphical Statics. Van Noostrand, New York (1878)
26. Levy, M.: La statique graphique et ses applications aux constructions. Gauthier-Villars Imprimeur-Librarie, Paris (1888)
27. Galassi, S., Misseri, G., Rovero, L., Tempesta, G.: Equilibrium analysis of masonry domes: on the analytical interpretation of the Eddy-Lévy graphical method. Int. J. Archit. Herit. **11**(8), 1195–1211 (2017)
28. Gerstener, F.: Handbuch der mechanik. Spurny, Prague (1831–1834)
29. O'Dwyer, D.: Funicular analysis of masonry vaults. Comput. Struct. **73**(1), 187–197 (1999)
30. Block, P., Ochsendorf, J.: Thrust network analysis: a new methodology for three-dimensional equilibrium. J. Int. Assoc. Shell Spatial Struct. **48**(155), 167–173 (2007)
31. Marmo, F., Rosati, L.: Reformulation and extension of the thrust network analysis. Comput. Struct. **182**, 104–118 (2017)
32. Avelino, R.M., Iannuzzo, A., Van Mele, T., Block, P.: Assessing the safety of vaulted masonry structures using thrust network analysis. Comput. Struct. **257**, 106647 (2021)
33. Pourfouladi, M., Pingaro, N., Valente, M.: PoliBrick plugin as a parametric tool for digital stereotomy modelling. Comput. Struct. **311**, 107722 (2025)
34. Paris, V., Olivieri, C., Adriaenssens, S.: The impact of construction on the structural design of a complex masonry curved shell. Int. J. Space Struct. **40**(2–3), 180–194 (2025)
35. Aita, D., Bruggi, M., Taliercio, A.: Limit analysis of masonry arches and domes with finite strength: funicular analysis versus stability area method. Meccanica **60**, 601–620 (2025)
36. Aita, D., Bruggi, M., Taliercio, A.: Thrust network analysis of masonry arches and domes of any stereotomy with finite compressive strength: multi-constrained minimization problem versus stability area method. In: Gabriele, S., Manuello Bertetto, A., Marmo, F., Micheletti, A. (eds.) Shell and Spatial Structures (IWSS 2023). Lecture Notes in Civil Engineering, vol. 437, pp. 150–160. Springer, Cham (2024)
37. Galassi, S., Ruggieri, N., Tempesta, G.: Ruins and archaeological artifacts: vulnerabilities analysis for their conservation through the original computer program BrickWORK. In: Aguilar, R., Torrealva, D., Moreira, S., Pando, M., Ramos, L.F. (eds.) Structural Analysis of Historical Constructions – An interdisciplinary approach, Proceedings of 11th International Conference on structural analysis of historical constructions (SAHC2018), RILEM bookseries 18, pp. 1839–1848. Springer International Publishing (2019)
38. Galassi, S., Ruggieri, N., Tempesta, G.: A novel numerical tool for seismic vulnerability analysis of ruins in archaeological sites. Int. J. Archit. Herit. **14**(1), 1–22 (2020)
39. Galassi, S., et al.: Digital survey and structural investigation on the triumphal arch of Caracalla in the archaeological site of volubilis in Morocco: retracing the timeline of collapses occurred during the 18th century earthquake. Int. J. Archit. Herit. **16**(6), 940–955 (2022)
40. Galassi, S., Zampieri, P.: A new automatic procedure for nonlinear analysis of masonry arches subjected to large support movements. Eng. Struct. **276**, 115359 (2023)
41. Di Pasquale, S.: Primo rapporto sulla Cupola di Santa Maria del Fiore. CLUSF, Firenze (1977)